

Halo bias in Lagrangian Space: Estimators and theoretical predictions

Chirag Modi^{1,2*}, Emanuele Castorina¹ and Uroš Seljak^{1,2}

¹*Berkeley Center for Cosmological Physics Campbell Hall 341, University of California, Berkeley CA 94720*

²*Department of Physics, University of California, Berkeley CA 94720*

Received ; in original form

ABSTRACT

We present several methods to accurately estimate Lagrangian bias parameters, in particular the quadratic terms, both the local and the non local ones and show the first clear evidence for the latter. Using Fourier space correlations, we also show for the first time, the scale dependence of the quadratic and non-local bias coefficients. We fit for the scale dependence of linear bias and demonstrate the validity of a consistency relation between linear bias parameters. Furthermore we employ real space estimators, using both cross-correlations and the Peak-Background Split argument. This is the first time the latter is used to measure anisotropic bias coefficients. We find good agreement among the methods, and also good agreement for local bias with $\text{ESP}\tau$ theory predictions. Possible relations among the different bias parameters are exploited. Finally, we also show how including higher order bias reduces the magnitude and scale dependence of stochasticity of the halo field.

Key words: cosmology: theory, large-scale structure of Universe – methods: analytical, numerical

1 INTRODUCTION

The distribution of Large scale structures (LSS) is one of the most important tools to study our Universe. With the recently concluded and upcoming LSS surveys such as BOSS¹, DESI², Euclid³, LSST⁴ etc. the vast amount of data will provide enough statistical power that errors in the analysis will be dominated by poor theoretical understanding of LSS. These surveys generally observe tracers such as galaxies, which unlike in weak lensing studies, do not perfectly trace the underlying matter density. Making this connection is a two step process- to realize that galaxies reside in collapsed dark matter halos following some statistical distribution- and that these halos themselves are biased tracers of matter distribution. In this paper, we focus on the latter of these and study novel techniques to measure halo bias. For a recent review on galaxy bias see Desjacques et al. (2016).

In full generality the relation between the halo density field and the dark matter contains information about all processes relevant for the formation of halos, as well as stochastic contributions arising due to the fact that halos come in

a finite number. However on large enough scales, we can hope to treat the problem perturbatively, and characterize the bias relation with a relatively small number of free parameters we can marginalize over. The simplest way to get physical intuition of halo bias comes from the so-called Peak-Background split argument (PBS) (Kaiser 1984; Kaiser & Cole 1989; Mo & White 1996; Sheth & Tormen 1999). In the original formulation of PBS, halos are regions where the value of the dark matter density field exceeds some critical threshold. This threshold can be crossed more easily in presence of a positive large scale dark matter fluctuations, and conversely less easily for a negative one. This means that, on average, overdense regions host more halos than the mean. Linear bias, b_1 , can therefore be defined as the linear response of the halo overdensity field, δ_h , to the presence of long wavelength perturbations, δ_m

$$\delta_h = b_1 \delta_m \quad (1)$$

The above relation can be generalized to any order in the density field, leading to the well known result by Fry & Gaztanaga (1993),

$$1 + \delta_h(x) = \sum_{n=0}^{\infty} \frac{b_n}{n!} \delta_m^n(x), \quad (2)$$

where however one must also enforce integral constraint by imposing that $\langle \delta_h \rangle = 0$.

Typically the bias expansion is written in two ways:

* E-mail: modichirag@berkeley.edu

¹ <https://www.sdss3.org/index.php>

² <http://desi.lbl.gov/>

³ <http://www.euclid-ec.org/>

⁴ <https://www.lsst.org/>

either by relating the the halo field to the dark matter field at time the observations are made, *i.e.* at low redshift, or by identifying in the initial Gaussian field regions which are more likely to collapse into halos at a later time. The former is called a Eulerian bias approach, the latter a Lagrangian bias approach. While the two approaches can be shown to be mathematically equivalent, each method has its own pros and cons.

It has been recently shown that the statistics of the halos does not only depend on the dark matter density field, as in Eq. (2), but also on spatial derivatives of the density field, (Desjacques et al. 2010; Musso et al. 2012; Baldauf et al. 2015) and on the tidal fields (Chan et al. 2012; Baldauf et al. 2012; Saito et al. 2014), each of which with its own new bias coefficient. These new terms, with abuse of notation, have been called non local bias coefficients, since they contain gradients of the the density field or of the gravitational potential. They have been shown to be important in the Eulerian approach (Chan et al. 2012; Baldauf et al. 2012; Saito et al. 2014), as they can be generated by non linear gravitational evolution, and can actually be predicted in Perturbation Theory (PT). As a matter of fact a complete basis would include all possible fields one can construct at any given order in perturbation theory compatible with the symmetry of the problem (McDonald & Roy 2009; Assassi et al. 2014; Senatore 2015; Mirbabayi et al. 2015; Fujita et al. 2016; Vlah et al. 2016).

The relevance of non local terms in the Lagrangian approach is still under debate. At the linear level, a scale dependent bias term is certainly present, as shown for instance in Desjacques et al. (2010); Paranjape et al. (2013a); Biagetti et al. (2014); Baldauf et al. (2015); Castorina et al. (2016a), using N-body simulations, and its measured value agrees fairly well with analytical models of structure formation (Paranjape et al. 2013a; Castorina et al. 2016a). At second order the leading non local term is proportional to the traceless shear s^2 , also called tidal field, defined as

$$s^2(\mathbf{x}) \equiv \sum_{ij} s_{ij}^2(\mathbf{x}), \quad s_{ij}^2(\mathbf{x}) = \left(\frac{\partial_i \partial_j}{\partial^2} - \frac{1}{3} \delta_{ij}^K \right) \delta(\mathbf{x}), \quad (3)$$

This new term has been measured in Eulerian space by Chan et al. (2012); Baldauf et al. (2012); Saito et al. (2014); Hoffmann et al. (2015), and it is nowadays included in all analysis of galaxy redshift surveys (Gil-Marín et al. 2015; Beutler et al. 2016; Sánchez et al. 2017). As we have already mentioned, a non-zero tidal bias is expected from non-linear gravitational evolution. It is therefore important to compare the values measured in N-body simulations to the assumptions of zero Lagrangian tidal bias, since an incorrect assumption on the latter could affect the determination of cosmological parameters. Tidal bias in the Lagrangian picture is non-zero if the shear is sampled around proto-halos differently than around random positions. We actually do expect the shear to play an important role in the process of halo collapse, that is very likely to happen in an ellipsoidal fashion (Bond & Myers 1996; Sheth & Tormen 1999; Desjacques & Smith 2008). The work in Sheth et al. (2013); Castorina et al. (2016a) have not shown clear evidence for tidal bias in Lagrangian space using N-body simulations. It is therefore interesting, and it is one of our main goals, to check whether this bias coefficient has non-zero value in a Lagrangian scheme and what would be the implications.

In addition to finding evidence of new bias coefficients, there is also another good reason to study Lagrangian halo bias. In Lagrangian Space it is more natural to write down relation among the different parameters, since, contrary to the Eulerian picture, non-linear evolution and the biasing scheme are decoupled from each other. For similar reasons, the evolution of bias with redshift, an important issue for galaxy surveys that spans a wide redshift range, is better understood in Lagrangian space. Finally, analytic approaches to predict the value of bias coefficients are built in the Lagrangian formalism, and can be used to put priors on some of the bias parameters. As we are ultimately interested in cosmological analysis of LLS data, a combination of priors and relations between the bias coefficients would be of great help to narrow the error bars on cosmological parameters.

Recently Vlah et al. (2016) have shown that at 1-loop in Lagrangian Effective Perturbation theory, the measurements in redshift space of the halo multipoles are very well described if one adopts the following bias expansion,

$$\delta_h(\mathbf{x}) = b_1 \delta(\mathbf{x}) + \frac{b_2}{2} [\delta^2(\mathbf{x}) - \langle \delta^2(\mathbf{x}) \rangle] + b_{s^2} [s^2(\mathbf{x}) - \langle s^2(\mathbf{x}) \rangle], \quad (4)$$

i.e. stopping at second order and assuming that third order terms are only generated by gravitational evolution. Our goal is to estimate the three bias coefficients in the above equation in N-body simulations using different techniques, and to compare them to analytic predictions. We are primarily interested in scale dependent bias, linear and non linear, and in the first clear evidence of tidal shear in the bias expansions. We will make use of three different estimators: cross correlations in Fourier Space, cross correlations in Real space, and direct implementation of the PBS argument to simulations.

We organize the paper as follows. In Section 2 we describe our approach to estimate bias using cross power spectra in Fourier space, showing results for the bias coefficients up to second order. In Section 3, estimators in real space that make use of the PDF of the density field are discussed, in particular focusing on their agreement with the Fourier space measurements. In Section 4 we present a direct application of PBS to simulations that allows to recover the value of the scale independent part of the bias coefficients. After establishing the agreement between different estimators, in Section 5, we present various relations amongst different parameters. Section 6 deals with the halo-bias stochasticity, and how much it is reduced by introducing a more complicated bias model. Finally, section 7 summarizes the main results, drawing conclusions and future prospects.

Since we work in Lagrangian space, throughout the text what we will refer to a dark matter halo as the initial collection of particles in the N-body simulations which a halo is made of at the final redshift, $z = 0$ let's say, *i.e.* the proto-halo.

The simulations we used for the analysis have been produced using the FastPM⁵ code (Feng et al. 2016). FastPM is a tool to generate non linear dark matter and halo fields in a quick way, employing a number of approximations to reproduce the results of full N-body simulation.

⁵ <https://github.com/rainwoodman/fastpm>

Despite its approximate nature, in Feng et al. (2016) it was shown that the code performs extremely well on various benchmarks such as dark matter power spectrum, the halo mass function and halo power spectrum. We refer the reader to Feng et al. (2016) for more details of the tests performed. We evolved 2048^3 particles in periodic cubic boxes of size 690, 1380 and 3000 h^{-1} Mpc. The mass of the particle in three cases is $3.37 \times 10^9 M_\odot/h$, $2.696 \times 10^{10} M_\odot/h$ and $2.77 \times 10^{11} M_\odot/h$ respectively. The linear power spectrum used was generated with CAMB with cosmology $h = 0.6711$, $\Omega_M = 0.3175$, $\Omega_b = 0.049$, $n_s = 0.9624$, and the initial particle displacement and velocity were computed at 2nd order in Lagrangian Perturbation Theory. The halos were identified using FOF halo finder in NbodyKit⁶ with the optimization presented in Feng & Modi (2016) using a linking length of 0.2. The smallest halo identified in every simulation consists of a 100 particles. We ran 5 independent realizations for every box and all the results presented are average of these runs. Unless stated otherwise, we show results at a single redshift, $z = 0$.

To calculate power spectra, we interpolate the halos on 512^3 grid using Cloud-In-Cell (CIC) interpolation and deconvolved the CIC window. To keep the comparison consistent, we used a 512^3 grid for dark matter density field as well and sampled the corresponding 512 modes from the 2048 modes available from the simulations.

2 BIAS ESTIMATION IN FOURIER SPACE

The easiest thing to measure in Fourier Space is linear bias,

$$b_1 = \frac{P_{hm}}{P_{mm}} \quad (5)$$

where in our notation the power spectrum between the X and Y field reads P_{XY} . In Figure 1, top panel, we show linear bias as measured from our FastPM runs for several halo mass bins. The common features shared by all the halos are: a constant piece on large scales, and then a k^2 -like piece on intermediate scales followed by a cut off, approximately at the scale of the halo. Similar plots for linear bias can be found for instance in Baldauf et al. (2015). A convenient parametrization of linear bias is therefore (Musso et al. 2012; Chan et al. 2015; Castorina et al. 2016a)

$$b_1(k) = \left(b_{10} + 2b_{11} \frac{d \log W(kR)}{d \log S} \right) W(kR) \quad (6)$$

where $S \equiv \sigma^2$ is the variance of the linear field smoothed on the scale of the halo R , $S \equiv (2\pi)^{-3} \int d^3k P(k) W(kR)^2$. For instance, for a Gaussian windows, $W(kR) = e^{-k^2 R^2}$, the scale dependent term b_{11} is exactly proportional to k^2 . In this form the two bias coefficients b_{10} and b_{11} are both dimensionless. Since neither the halo scale, R , nor the average halo shape, $W(kR)$, are known, fitting the above equation to the simulations results requires some care. To be conservative, and for comparison with previous work, we assume proto-halos of mass M are spherical patches of size $R = (4\pi/3\rho_m M)^{1/3}$, such that the window function $W(kR)$

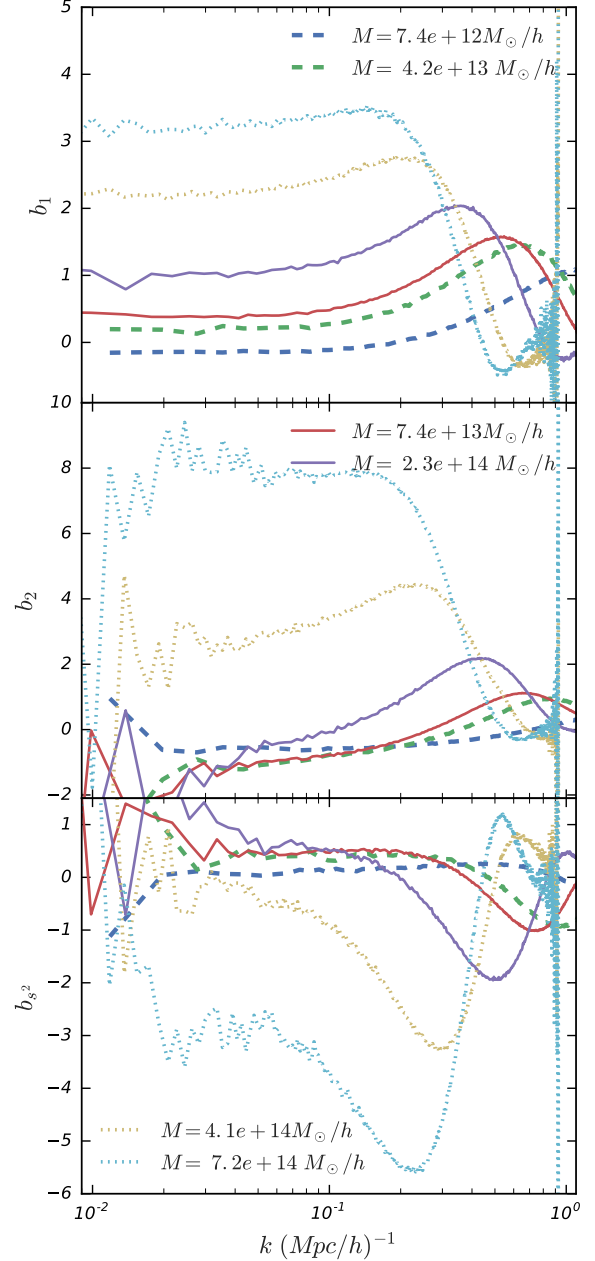


Figure 1. Bias parameters as function of k : We show b_1 , b_2 and b_{s2} as measured from Fourier space estimator. The dashed, solid and dot-dashed lines are from different boxes of size, $L = 690, 1380, 3000$ Mpc/h, respectively. For clarity, we have refrained from showing all the mass-bins. The dependence on the wavenumber is the shared by all the parameters: constant piece on large scales followed by k^2 -like piece on intermediate scales followed by a cutoff around the halo scale.

⁶ <https://github.com/bccp/nbodykit>

is top-hat of radius R in real space. As a further safeguard, we fit for $b_1(k)$ only upto the first peak near the halo scale, after which the halo window function starts to dominate over the scale dependence of bias.⁷ At this time we can fit for the scale independent piece of linear bias, b_{10} , as well as for the scale dependent one, b_{11} , in Eq. (6). A comparison of b_{10} with theoretical models and with other estimators for linear bias on large scales will be done in the next section, whereas here we only show, in Figure 2, results for b_{11} as a function of mass and how it compares to the analytic prediction shown as the continuous line. The model we use is an extension of Peaks theory (BBKS)(Bardeen et al. (1986)) that includes the Excursion set constraints (ESP) (Musso & Sheth 2012; Paranjape et al. 2013a) and a simple treatment of ellipsoidal collapse (ESP τ) (Castorina et al. (2016a)). The ESP τ model reproduces reasonably well the halo mass function and linear and quadratic bias halo bias on large scale as measured from N-body simulations, see Castorina et al. (2016a) for more details. It has one free parameter, β , entering the definition of the critical threshold, B , required for collapse, which measures the relative importance of shear fluctuations to density fluctuations at the halo scale

$$B = \delta_c + \beta\sqrt{s^2} \quad (7)$$

where $\delta_c = 1.686$ is the standard spherical collapse value. We fit β by eye to the measurements, finding that $\beta = 0.3$ provides a good fit to the data. ESP τ performs remarkably, if not surprisingly, well in comparison to the scale dependent piece over a 3 orders of magnitude in mass. Since the value of scale dependent bias is sensitive to the choice of the filter (see Eq. (6)), the agreement between the theory and the data suggests that defining proto-halos with a Top-Hat filter is a very good approximation. This finding is in contradiction with Chan et al. (2015), and it deserves future investigation in a future work. As we will see later in Section 5 the performance of ESP τ on scale dependent bias is important, as the value of b_{10} and b_{11} are related by mass conservation.

We would like to extend the results we have shown for b_1 to higher order bias coefficients, in particular we seek for a simple estimator of b_{s^2} . First, notice that, since the bias relation in Eq. (4) is written in real space, any estimators of second order bias coefficients in Fourier space will make use of convolutions, for instance the squared density field is trivially

$$\delta^2(x) = \int \frac{d^3k}{(2\pi)^3} e^{-i\mathbf{k}\cdot\mathbf{q}} \int d^3q \delta(q)\delta(k-q) \quad (8)$$

and an analogous expression holds for s^2 . We also remind that since the dark matter field is linear in Lagrangian space, cross correlations between the halos and a generic quadratic fields are very easy to write down, as any expectation value involving three fields vanishes. Within the model in Eq. (4)

we arrive to

$$P_{h\delta^2}(k) = \frac{b_2(k)}{2} P_{\delta^2\delta^2}(k) + b_{s^2}(k) P_{s^2\delta^2}(k) \quad (9)$$

$$P_{hs^2}(k) = \frac{b_2(k)}{2} P_{s^2\delta^2}(k) + b_{s^2}(k) P_{s^2s^2}(k)$$

where for instance

$$P_{\delta^2\delta^2}(k) = k^3 \int_{r=0}^{\infty} \int_{x=-1}^1 \frac{dr dx}{4\pi^2} P(kr) P(k\sqrt{1+r^2-2rx}) \quad (10)$$

and similar expression involving Legendre polynomials can be written for $P_{s^2\delta^2}(k)$ and $P_{s^2s^2}(k)$.

The linear system of equations in Eq. (9) can be solved to obtain a value of b_2 and b_{s^2} at each mode k and for different halo populations. (To assist in solving, one can also re-write these equations in terms of $g^2 = s^2 - \frac{2}{3}\delta^2$ to decouple s^2 from δ^2 , though it is not necessary.) The solution is shown in the two bottom panels of Figure 1, which makes clear that the behavior as a function of k we have seen for linear bias also applies to higher order bias coefficients. Scale dependence of non linear bias would have, for instance, to be taken into account for Lagrangian Perturbation theory calculations beyond 1-loop order.

The bottom panel clearly shows that tidal bias is non zero for a variety of halo populations. This has important consequences for cosmological analyses using Lagrangian perturbation theory plus Lagrangian bias (Matsubara (2008); Carlson et al. (2013); Wang et al. (2014); White et al. (2015); Vlah et al. (2016)). As already known, b_2 is negative for low mass halos and then becomes large and positive for very massive halos. The opposite trend is observed for b_{s^2} , which is negative at the high mass end. This is expected, since shear is acting against the formation of the halos, whereas density enhances it. Had we started with a local bias expansion we would have gotten different results for $b_2(k)$, in contradiction with the results of the next sections, and as further discussion at the end of Section 3.

While we do find evidence for non-zero tidal bias, getting the precise values for various mass bins is non-trivial. This is due to the combined effect of cosmic variance as well as degeneracy between δ^2 and s^2 on large scales, making things noisy on very large scales where the scale independent piece of bias should dominate, and it becomes more severe for our smallest simulation box. This also comes into play when we try to extend this method to b_3 (see Appendix A). Furthermore, unlike b_1 , the functional form of the scale dependence of b_{s^2} is highly non-trivial (Matsubara 2008; Musso et al. 2012), and hence much more sensitive to the halo window, which is not exactly known, as well as k_{max} , up to which any such a fit is done. Nevertheless, for the purpose of this work, we strive to fit for a constant on large scales as function of increasing k_{max} and choose the value which gives the best reduced χ^2 of the fit.

3 REAL SPACE BIAS ESTIMATORS

Cross correlations between the halos and other fields can also be written in real space. The advantage of working in Lagrangian Space is that we know the PDF of the density field, and therefore estimators for the cross correlation and

⁷ The fact that linear bias in Figure 1 crosses zero at large k excludes the Gaussian window, $W_G = e^{-k^2 R^2/2}$, employed by Baldauf et al. (2015). The choice of the filter is almost irrelevant for the best-fit value of b_{10} .

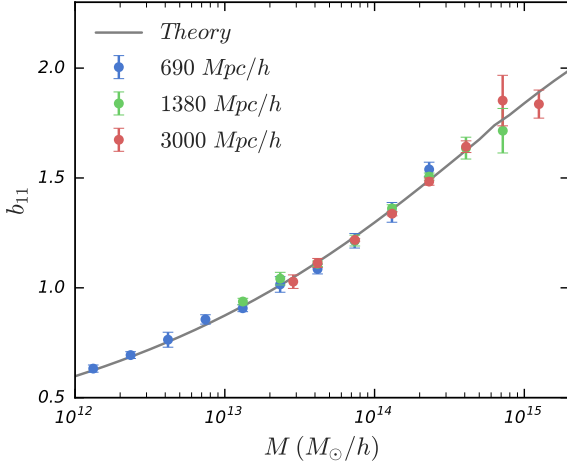


Figure 2. b_{11} as a function of mass: The values are estimated from the best fit values for b_1 and using Eq. (6), assuming a tophat window $W(kR)$ at the halo scale. We will also follow the scheme of the colors blue, green and red (B, G, R) representing different box sizes throughout this paper unless explicitly mentioned otherwise, or when the box size is not important.

for the bias coefficients can be written down without expensive pair counting. Following (Szalay 1988; Musso et al. 2012; Paranjape et al. 2013b; Biagetti et al. 2014; Castorina et al. 2016b), if Δ_0 is the dark matter density in a sphere of radius R_0 around halos of given mass M , for the n -th order bias coefficient we can write

$$\hat{b}_n = \frac{S_\times^n}{S_0^{n/2}} \frac{1}{N} \sum_{i=1}^N H_n \left(\frac{\Delta_{0i}}{\sqrt{S_0}} \right) \quad (11)$$

where the sum runs over all the N halos falling into the mass bin, and $H_n(x)$ is a probabilist's Hermite polynomial. The rationale behind this estimator is that Hermite Polynomials are orthogonal polynomials of Gaussian random fields, therefore they will pick up only the n -th order in the density field contribution to the bias expansion. In the above equation $S_0 = \sigma^2(R_0)$ is the variance of the field on large scale, and $S_\times = \sigma^2(R, R_0)$ is the cross variance between the halo scale and the large scale.

In real space, the convenient separation of scales we have seen in Fourier space is lost. The scale independent and the scale dependent term will now be mixed in the estimator in Eq. (11). By Fourier transforming Eq. (6), it is easy to see that measurements in real space can be fitted by

$$b_1 = b_{10} + \epsilon_\times b_{11} \quad (12)$$

where $\epsilon_\times = d \log S_\times / d \log S_0$. The scale independent piece can be extracted by using a very large R_0 , since ϵ_\times goes to zero at large scales, or by combining measurements at different scales (Paranjape et al. 2013b; Castorina et al. 2016b). Our first goal is to compare estimates of b_{10} and b_{20} from real and Fourier space. We find that both approaches give very similar results. In Figure 3 we compare the values of linear and quadratic bias estimated from real space (squares and triangle) and Fourier space (circles). The agreement between the two is very good over the whole mass range we probe and it is very well described by ESP τ . It is important

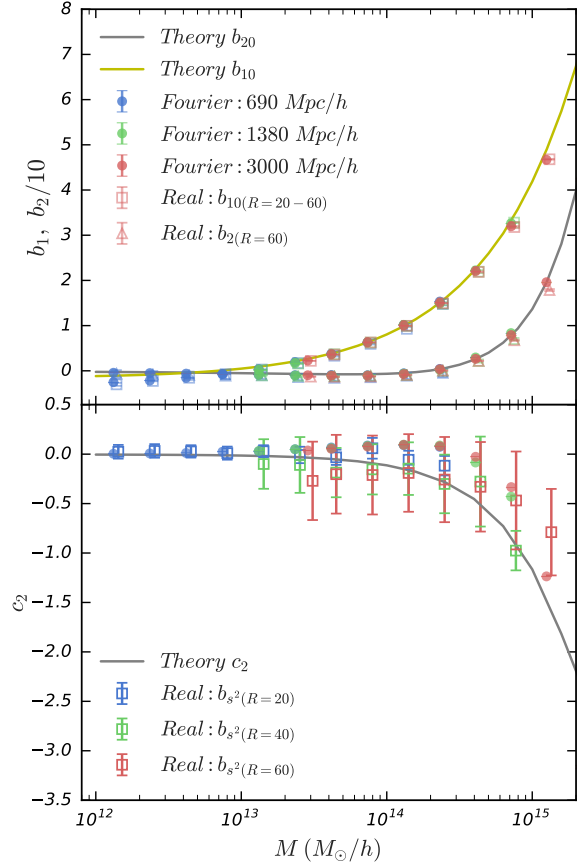


Figure 3. Bias estimators b_1 , b_2 and b_{s^2} as function of mass: agreement between real space, Fourier space estimator and ESP τ theory. For real space, we mention in the subscript the large scale used to calculate the bias parameters. For b_{10} , we use Eq. (12) and the two smoothing scales mentioned to extract scale independent part. Real space points have been shifted along x -direction for clarity.

to point out what would have happened if we had not include shear in our bias estimator in Fourier space. This is shown in Figure 4, in which the estimates of b_2 in Fourier space without taking shear into account are clearly incompatible with the real space results (and with the theoretical model).

We conclude the discussion of real space bias measurements by generalizing the estimator in Eq. (11) to non local bias parameters. It is easy to show that the shear field, s^2 , is χ^2 -distributed with five degrees of freedom (Bond & Myers 1996; Sheth et al. 2001, 2013; Castorina et al. 2016b), which implies that the orthogonal polynomials to use in the estimator are Laguerre polynomials,

$$\hat{c}_2 = -\frac{1}{r^2} \frac{1}{N} \sum_{i=0}^N L_1^{3/2} \left(\frac{5s_{0,i}^2}{\langle 2s_0^2 \rangle} \right) \quad (13)$$

where $r = S_\times / \sqrt{S S_0}$ and s_0 is the large scale (R_0) shear. This estimator assumes that the bias expansion is written

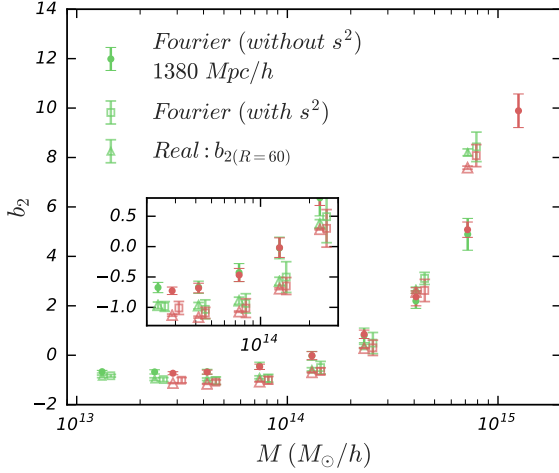


Figure 4. $b_2(M)$ **without** b_{s2} : Fourier space estimator for b_2 with (empty boxes) and without (solid dots) including the shear in Eq. (9). For comparison the real space estimates (triangles), by construction independent of the shear, is shown. The two estimators are in agreement only allowing a non-vanishing tidal bias in Fourier Space. Though not shown here, the fit for b_2 without shear is also much worse for PBS estimator, especially for high mass halos. Overall consistency with real space estimates is presented in Figure 3.

in terms of Laguerre polynomials,

$$1 + \delta_h(M) \supset \tilde{c}_2 L_1^{3/2} \left(\frac{5s^2}{\langle 2s^2 \rangle} \right) \quad (14)$$

which are properly normalized and ensure by construction that $\langle \delta_h \rangle = 0$. The bias parameter c_2 is related to the previously defined tidal bias by the following relation,

$$b_{s2} = \frac{15}{2} c_2 \quad (15)$$

and from now on, to reduce the dynamic range in the figures, we will plot only $c_2 = \tilde{c}_2/\sigma^2$ (we will make use of the words c_2 , and b_{s2} interchangeably). Figure 3, bottom panel, shows the large scale values of the b_{s2} estimated from real and Fourier space. The two agree fairly well, however the real space measurements have still significant errorbars that do not allow us to assert the significance of the excursions of b_{s2} above zero we see in Fourier Space. We plan to come back to this issue, with better measurements, in a future work. The analytic prediction for the tidal bias is shown as solid line in Figure 3. The agreement with the measurement in the N-body is poorer than for $b_{1(2)}$ and it indicates that, although, the model in Castorina et al. (2016a) is capable of capturing the gross features of shear into the bias expansions more work is needed to properly understand the origin of the non local bias parameters.

4 PBS ESTIMATOR

The very first definition of halo bias, the PBS, says that bias parameters are the n -th order response of the halo population to the presence of large scale fluctuations. For the case of isotropic response, one can exploit the well known equivalence between a infinite wavelength spherical perturbation

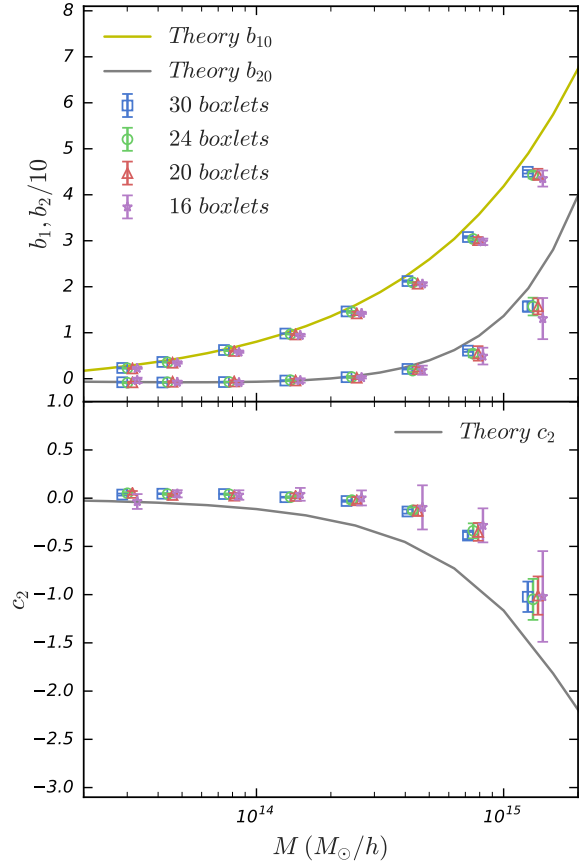


Figure 5. PBS bias measurements from different boxlet sizes: As explained in the text, the size of error bars increase with increasing boxlet sizes (decreasing number of boxlets). Markers are shifted along x-direction with decreasing numbers of boxlets for clarity.

in a flat Friedmann-Robertson-Walker (FRW) background and a closed FRW Universe. This technique, known as Separate Universe, allows to measure isotropic bias parameters in N-body simulations with basically no cosmic variance (McDonald 2003; Sirko 2005; Wagner et al. 2015; Lazeyras et al. 2016; Li et al. 2016; Baldauf et al. 2016). The drawback of this method is that it does not apply to tidal bias, where one would need N-body simulations with anisotropic expansion along the different axis, since the introduction of shear breaks isotropy of space.

In Lagrangian space, where the density field is linear, one can take advantage of the PBS to measure *any* bias parameters in a much simpler way. Consider a relatively large box (of size L) of a N-body simulation. We chop this box into several smaller boxes of linear size l , we call them boxlets. Each boxlets will have its own value of density field, drawn from a Gaussian distribution smoothed at the scale of the boxlet, R_b (this scale is computed by matching the volume of a sphere of radius R_b and a cube of the boxlet side l). In order to suppress scale dependent terms one must ensure that $R/R_b \ll 1$, where R is the typical size of halos. Differently from the standard Separate Universe approach,

each boxlets will also have its own value of the shear field, drawn from a χ^2 -distribution.

To estimate the density associated with every boxlet, we smooth the box with a tophat window of the scale of the boxlet, R_b . The value of this smoothed density field at the center of every boxlet is the associated super sample density mode with boxlet (δ_i). For this smoothed density field then, we estimate the shear field over the whole box using Eq. (3). The value of this shear field at the center of every boxlet is the associated super sample shear value (s_i^2). Since the smoothing scale is large and hence the variance is small, the value of these fields at the center of the boxlet is equivalent to computing the mean from all the grid cells belonging to each boxlet.

To evaluate the halo overdensity in every boxlet, we measure the mean number of halos in the box (\bar{N}) and in every boxlet (N_i), and then compute the relative excess in halo number density as

$$\hat{\delta}_{h_i} = \frac{N_i/l^3 - \bar{N}/L^3}{\bar{N}/L^3}. \quad (16)$$

Bias parameters can then easily be obtained by fitting the above quantity to the measured density and shear in each boxlet

$$\hat{\delta}_{h_i} = b_{10}\delta_i + \frac{1}{2}b_{20}\delta_i^2 + b_{s2}s_i^2 + \dots \quad (17)$$

While this method has several advantages over standard techniques it has its own drawbacks. Since the boxlets are large, $\mathcal{O}(100) h^{-1} \text{Mpc}$, the value of the density and shear are small and the scatter among different boxlets large. This makes difficult to fit for bias parameters and it yields slightly larger error bars than the standard Separate Universe technique. Also, high mass halos are poorly sampled on the small volume of the boxlets, and are mostly affected by non-poissonian shot noise, which is hard to estimate.

Figure 5 shows bias coefficients estimated using Eq. (17) for different chopping of the $L = 3000 h^{-1} \text{Mpc}$ box, $L/l = 30, 24, 20, 16$. For various size of the boxlets the measured bias parameters agree among themselves, and we also report clear evidence of tidal bias with this novel estimator. As discussed, the size of error bars decreases with decreasing the size of boxlets (increasing number) due to better constraining power. However, to safe-guard against possible systematic errors, we will henceforth quote values for $L/l = 20$ in the remainder of this work.

The concordance between the three different estimators used in this paper, Fourier Space, real space and PBS, is shown in Figure 6 and it is one of our main results. We stress that, similarly to what happened in Fourier Space, in fitting Eq. (17), the presence non local bias was crucial to obtain the agreement for local linear and quadratic bias between different estimators, as well as the theory. While we do find convincing evidence of tidal bias in all three measurements and there is general agreement in the values, a % level calibration of non local bias would require more simulations and better control of any systematics, and it goes beyond the scope of this paper. We plan to return to it in a future work.

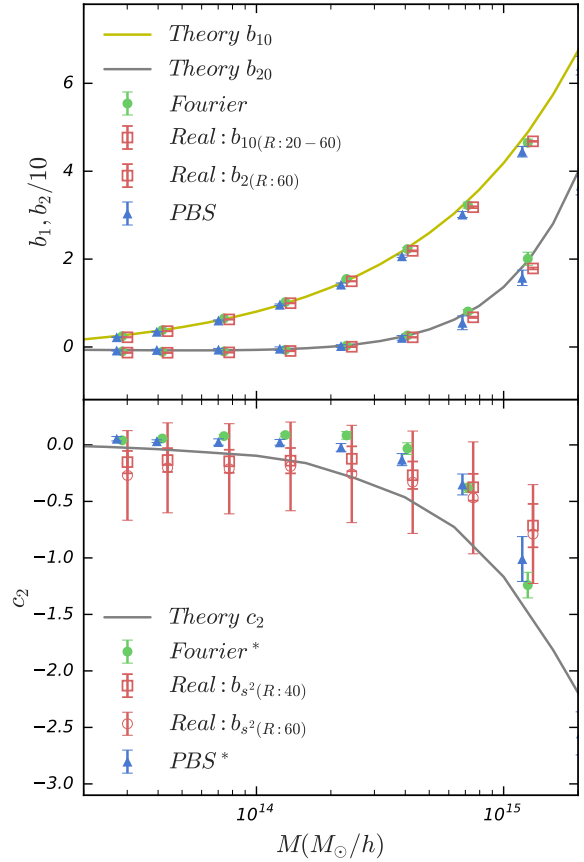


Figure 6. PBS b_1 , b_2 and b_{s2} as function of mass: comparison with ESPTau theory, fourier space and real space measurements. Measurements are shown only for 3 Gpc/h box and PBS measurements for 20 boxlets. The PBS and real space points have been shifted along x-direction for clarity.

5 RELATIONS AMONG THE BIAS PARAMETERS

Relations among the bias coefficients are of great value for cosmological analyses as they make possible to reduce the number of free parameters. In this section we study three kinds of such relations: between the the scale dependent and the scale independent terms of linear bias, the general universality of these parameters with redshift and empirical relations between b_2 or b_{s2} and b_1 that universality allows one to fit for.

5.1 Consistency relation for linear bias

In the Lagrangian picture, properties of the (proto-)halos profiles are closely related to the bias parameters. From the very definition of halo mass and halo bias in Eq. (12), it is easy to see that at the scale of the halo $\epsilon_\times(R) = 1$, and therefore (Musso et al. 2012; Paranjape et al. 2013a; Paranjape et al. 2013b; Castorina et al. 2016a,b)

$$b_{10} + b_{11} = \frac{\langle \delta_{1\times} \rangle}{\sigma^2} \quad (18)$$

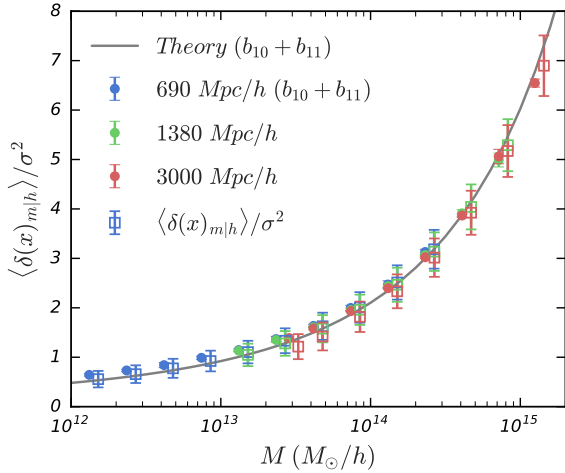


Figure 7. Consistency Relation between b_{10} and b_{11} : Eq. (18) relates the linear bias to the mean dark matter overdensity at the position of the halos. For Spherical collapse, this mean $\langle \delta(x)_{m|h} \rangle = 1.686$, but it is a function of mass in Ellipsoidal collapse. The square markers (shifted along x-direction for clarity) are the direct measurements from the simulations while solid dots are prediction from bias parameters estimated from Fourier space correlations in previous sections from those catalogs.

where $\langle \delta_{1x} \rangle$ is the mean dark matter density inside halos of a given mass and σ^2 is the variance on the scale of halos. If halos were perfect spheres, then $\langle \delta_{1x} \rangle = \delta_c = 1.686$. Measurements of this quantity have been presented in Sheth et al. (2001); Dalal et al. (2008); Robertson et al. (2009); Ludlow et al. (2013); Despali et al. (2016); Castorina et al. (2016a). The above equation says something very non-trivial about bias coefficients: one can measure the value of bias parameters at large scales and learn something about the density of halos at a much smaller scale, the halo scale. It is also important to note that Eq. (18) remains valid even in the presence of assembly bias, as it is a direct consequence of the definition of mass (Castorina et al. 2016b). We have seen in Figure 2 and Figure 3 that different estimates of linear bias agree with each other and with a theoretical model. We thus expect the consistency relation to hold in the data and to be well described by the $\text{ESP}\tau$ model. This is shown in Figure 7, where one can see how the Eq. (18) is verified at the level of the data, blue and red points with error bars, and how the theory actually does a good job in predicting it. In real space it is much harder to check the consistency relation for linear bias, see Castorina et al. (2016a), while a similar analysis in Fourier space can be found in Chan et al. (2016) (in preparation). Since the k^2 term in linear bias, b_{11} , is highly degenerate with the leading order counter term α , in the Effective Field Theory (EFT) of Lagrangian perturbation theory (Vlah et al. 2016), one could argue that it should be possible to just fit for b_{11} in a EFT approach, and then use the consistency relation to put a prior on the value of scale dependent bias. Similar relation should hold between higher order bias parameters and higher moments of the density field at the halo scale.

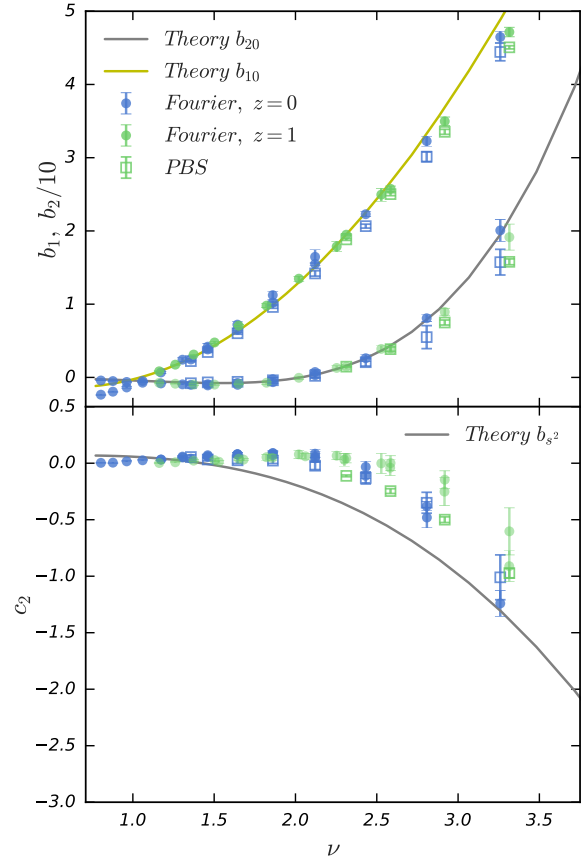


Figure 8. Universality of bias parameters: agreement between our Fourier space and PBS estimator across the redshifts, blue points are from $z = 0$ and green points are $z = 1$. Fourier space points are for all three boxes while PBS measurements are only for 3 Gpc/h box. The analytic prediction is assumed to be redshift independent.

5.2 Universality of Bias Relation with redshift

In the study of halo abundances and clustering, universality means that the halo mass function and halo bias are unambiguously determined by a single function of cosmology and redshift, the variance of the linear density field, $\sigma(z)$. The existence of universal relations is important, since it means we have a proxy for how the bias of a population of halos evolves, for instance, with redshift. Violations of the universality of the mass function in N-body simulations with redshift have been reported in Tinker et al. (2008); Crocce et al. (2010); Watson et al. (2013), while the Eulerian linear bias remains a universal function (Sheth & Tormen 1999; Tinker et al. 2010; Hoffmann et al. 2015). The purpose of this section is to test universality of linear and non linear local bias, as well as the novel b_s^2 , with redshift. The best way to test universality is to plot quantities estimated at different redshift as function of the peak height $\nu = 1.686/\sigma$.

We carried out the analysis of the previous Sections at $z = 1$, and a test of universality of bias is reported in Figure 8. The values of b_1 and b_2 , in blue at $z = 0$ and in green at $z = 1$ in the top panel, align very nicely as a function of ν

over all the mass range probed by our simulations. For tidal bias, the PBS measurements do show that the bias is approximately universal, whereas the Fourier space measurements show some disagreement for large mass halos. While this can possibly be due to poor fits, as discussed in Section 2, on the other hand, in the $\text{Esp}\tau$ model, the amplitude of the tidal bias is mainly set by the parameter β appearing in Eq. (7), which a priori could have arbitrary redshift dependence. The continuous line is the same $\text{Esp}\tau$ theory, for which we assume that β does not depend on redshift. A detailed study of the importance of the shear for halo formation as a function of redshift goes beyond the scope of this work, and we intend to come back to this issue in the future.

5.3 Relation between higher order bias parameters

Another way to restrict the dimensionality of the bias parameters space is to find relations between linear bias and higher order bias parameters. While such relations can be determined at each redshift, if the bias parameters are universal, then one could just fit for $b_2(b_1)$ and $b_{s2}(b_1)$. In an Eulerian framework this has been discussed a lot in the literature, see recent work by Hoffmann et al. (2015, 2016); Lazeyras et al. (2016). However it is important to realize that if such relations exist, they do because they hold in Lagrangian Space. We must also stress another word of caution: the nature of these relations is empirical, not fundamental, and it is, for instance, violated by assembly bias effects. Figure 9 shows b_2 as a function of b_1 , upper panel, and b_{s2} as a function of b_1 , lower panel. Since the PBS estimates of tidal bias are universal, we show the relations only for these data. The measured values smoothly align, indicating that the relation could be fitted by some simple functional form. As expected from results in the previous sections, the theory is able to predict very well the relation between non linear and linear bias, but it is not as accurate for the tidal bias.

We want now to go back to the relation between Lagrangian and Eulerian bias parameters as discussed in the Introduction. If b_{s2} was zero, gravitational evolution makes a unique prediction for the Eulerian tidal bias, b_{s2}^E , (Chan et al. 2012; Baldauf et al. 2012)

$$b_{s2}^E = -\frac{2}{7}b_1 = -\frac{2}{7}(b_1^E - 1) \quad (19)$$

where we have used the well known relation $b_1^E = 1 + b_1$. As we have measured a non-zero shear bias in Lagrangian space, the above equation needs to be modified (Sheth et al. 2013),

$$b_{s2}^E = b_{s2} - \frac{2}{7}(b_1^E - 1) \quad (20)$$

Figure 10 shows the relation between linear and tidal bias in Eulerian space, using the measurement from the PBS method. The assumption of no Lagrangian shear bias, black line, is far from the measurements at both low and high value of b_1^E . Thus, in the presence of this Lagrangian shear bias, using the relation of Eq. (19) such as done in analysis of Gil-Marín et al. (2015); Beutler et al. (2016); Sánchez et al. (2017) can lead to possible systematic errors in the analysis. Since the analytic model does not yield an accurate fit to

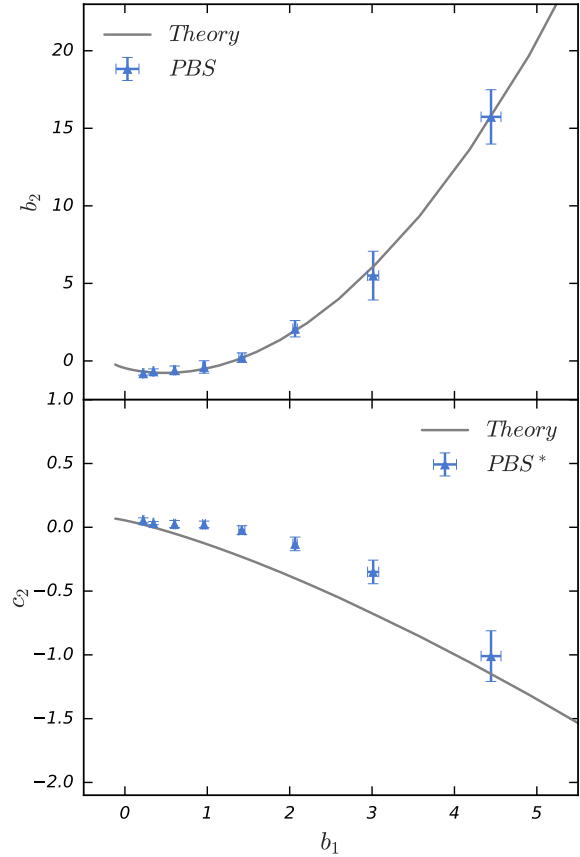


Figure 9. Relation between bias parameters: Empirical relations between $b_2 - b_1$ (upper panel) and $b_{s2} - b_1$ (lower panel) shown only for PBS estimator since tidal bias is most universal for these. The solid lines are using bias values predicted by $\text{Esp}\tau$ theory. These relations, co-evolved to Eulerian space help to reduce dimensionality of bias parameter space.

the data, for practical purposes we provide a numerical fit to the PBS measurements:

$$b_{s2}^E(PBS) = 0.64 - 0.3b_1^E + 0.05(b_1^E)^2 - 0.06(b_1^E)^3 \quad (21)$$

6 STOCHASTICITY

Following Seljak & Warren (2004); Hamaus et al. (2010); Baldauf et al. (2013), for any two fields X and Y , where the field Y is supposed to model field X , we measure the error in modeling in terms of the stochasticity, S_{XY} , defined as

$$S_{XY} = P_{XX} - \frac{P_{XY}^2}{P_{YY}}. \quad (22)$$

For our purpose here, we are interested in examining how well we reconstruct the halo field with the estimated bias parameters. Thus P_{XX} is the halo power spectrum (P_{hh}), while P_{YY} is the auto-power spectra for the biased field

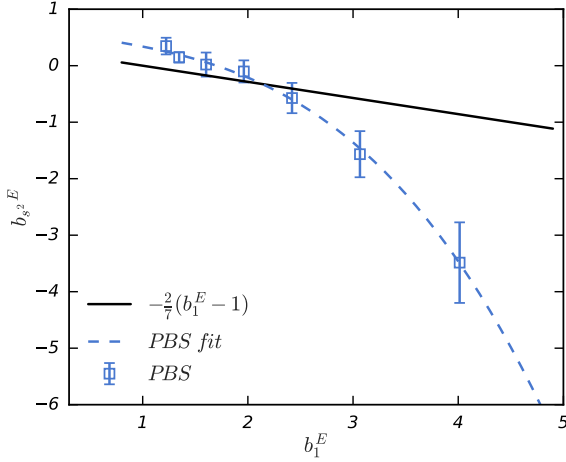


Figure 10. Eulerian Non-Local bias: Comparison of the evolution relation for shear bias in Eulerian space with (Eq. (20); markers) and without (Eq. (19); solid black line) the presence of Lagrangian shear bias as measured by PBS estimator. The numerical best fit (Eq. (21)) to the measurement points is in dashed blue.

(P_{bb}). The explicit expression in terms of bias parameters is

$$P_{XY} \equiv P_{hb} = b_1 P_{h\delta} + \frac{b_2}{2} P_{h\delta^2} + b_{s^2} P_{hs^2} \quad (23)$$

$$P_{YY} \equiv P_{bb} = b_1^2 P_{\delta\delta} + \frac{b_2^2}{4} P_{\delta^2\delta^2} + b_{s^2} P_{s^2s^2} + b_2 b_{s^2} P_{\delta^2s^2}$$

If the bias-field reconstructs the halo field perfectly, all the three power spectra in the definition of stochasticity should be the same resulting in $S_{hb} = 0$. However since the number of halos, n , is finite, the halo auto spectrum contains Poisson shot noise, $\frac{L^3}{n}$ (where L is the box size), which is not captured by the continuous bias field.

In Figure 11, we show measurement of stochasticity in Eq. (22) for three different mass bins, one from each of the three simulation boxes. For each mass, we show how the stochasticity changes as we include higher order bias parameters over simple linear bias b_1 in Eq. (23). To make this Figure, we again averaged over the stochasticity of 5 simulations for a given size and for each simulation, and we used the same mean value, across the realisations, of the bias coefficients, which in this case was the constant (large scale) Fourier space bias.

Overall, on large scales, the stochasticity is close to its Poisson shot noise value for intermediate and low mass bin, while its somewhat lower for heavier halos (Baldauf et al. (2013) explains this as exclusion effects). However, especially for the low mass halos, simply using the linear bias for halo field does leave significant scale dependence in the stochasticity which is improved upon by including higher order bias parameters (upper panel). This is useful since this residual can still be modeled with a scalar, if not necessarily poisson, shot noise. In addition, including b_2 and especially b_{s^2} does assist in reducing stochasticity further over linear bias models (lower panel).

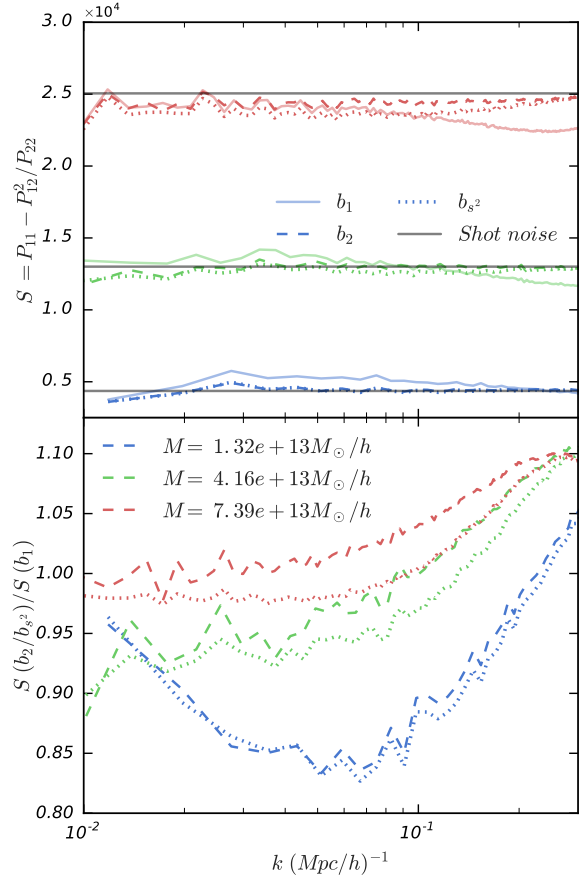


Figure 11. Stochasticity of Halos: The stochasticity in the upper panel is calculated using Eq. (22). The solid lines, dashed and dotted lines respectively correspond to measurements on successively including b_1 , b_2 and b_{s^2} in Eq. (23). For comparison, the black lines are shot noise for that mass bin. The lower panel shows the ratio of dashed and dotted lines of upper panel with the solid lines to emphasize that more complex bias models reduce stochasticity.

7 DISCUSSION AND CONCLUSIONS

Understanding the relation between the galaxy or halo field and the underlying dark matter distribution, is crucial in order to extract cosmological information from the LSS.

In this paper we have focused our attention to halo bias defined in Lagrangian Space. We employed three different estimators of bias parameters- Fourier space correlations, real space correlations and PBS estimator. The three approaches are quite different and thus sensitive to different systematic effects, nevertheless their agreement in terms of best-fit bias parameters as a function of halos mass is quite remarkable (Figure 6).

We have shown a convincing evidence for shear bias in Lagrangian space with all three methods (Figures 1, 3 and 6). Indeed, including the tidal bias was crucial to obtain the consensus of quadratic local bias of all the three estimators (Figure 4). We have shown that the model presented in Cas-

torina et al. (2016a) is able to predict well b_1 and b_2 , but it misses a good description of tidal bias.

The Fourier space estimator have also enabled us to present the scale dependence of quadratic and shear bias (Figure 1), and to show that it is similar to the one of linear bias. For linear bias, the Fourier space method allowed us to check that the scale dependent piece (Figure 2) is very well predicted by theory. This has implications for the problem of what is the right window to use when defining halos in Lagrangian space. We also successfully demonstrated, in N-body simulations, the validity of a consistency relation for linear bias coefficients, 18 and Figure 7, that are fundamental to the bias parameters. This opens the door to reduce the number of independent bias parameters.

We have then used the PBS argument to generalize previous results on bias with respect to density, to the case of bias with respect to the shear field. We were therefore able to measure non-local bias as the response of the halo number density to the presence of long wavelength tidal field (Figure 5). In the appendix A, we also show that this method can be extended to third order bias parameter b_3 (Figure A1). However care needs to be taken while choosing the size of boxlets due to the dichotomy between better constraining power for small boxlets but at the possible cost of residual scale dependence and non-Poissonian shot noise.

Relations among linear bias and quadratic bias parameters have also been discussed, with the general finding that those relations exist and can be easily fitted for (Figure 9). Along the way we also showed that all these bias parameters are to a very good approximation a universal function of redshift (Figure 8).

We note that while the evidence of non-zero tidal bias seems convincing and there is general agreement between different estimators, Fourier space shear estimates make larger excursions above zero than real space or PBS estimates (Figure 6), and also seem to exhibit some violations of universality for high mass halos. While there is no a priori reason to expect density and shear bias coefficients to exhibit the same level of universality, we discussed in Section 2 whereas the possible reason could be poor fits due to lack of correct halo window as well as complicated scale dependence of tidal bias, coupled with degeneracy of δ^2 and s^2 on very large scales. This is an important point which we wish to investigate in future work, with better measurements.

As we have shown, the analytic model in Castorina et al. (2016a) is not capable to reproduce our measurements of the tidal bias, Figure 10, therefore we provide a numerical fit to the relation between the Eulerian linear bias, b_1^E , and the Eulerian shear bias, $b_{s^2}^E$, in Eq. (21).

Finally, we discuss the stochasticity of the halo field and find that including more complex bias models over simple linear bias does seem to reduce stochasticity, especially its scale dependence (Figure 11). This makes these models worth studying since a scale independent stochasticity can be parameterized with a constant shot noise which can be marginalized over in the analysis.

ACKNOWLEDGMENTS

EC would like to thank Ravi Sheth, Aseem Paranjape and Martin White for useful discussions. This work is supported by NASA grant NNX15AL17G.

REFERENCES

- Assassi V., Baumann D., Green D., Zaldarriaga M., 2014, *J. Cosmology Astropart. Phys.*, **8**, 056
- Baldauf T., Seljak U., Desjacques V., McDonald P., 2012, *Phys. Rev. D*, **86**, 083540
- Baldauf T., Seljak U., Smith R. E., Hamaus N., Desjacques V., 2013, *Phys. Rev. D*, **88**, 083507
- Baldauf T., Desjacques V., Seljak U., 2015, *Physical Review D*, **92**, 123507
- Baldauf T., Seljak U., Senatore L., Zaldarriaga M., 2016, *J. Cosmology Astropart. Phys.*, **9**, 007
- Bardeen J. M., Bond J. R., Kaiser N., Szalay A. S., 1986, *The Astrophysical Journal*, **304**, 15
- Beutler F., et al., 2016, preprint, ([arXiv:1607.03150](https://arxiv.org/abs/1607.03150))
- Biagetti M., Chan K. C., Desjacques V., Paranjape A., 2014, *Monthly Notices of the Royal Astronomical Society*, **441**, 1457
- Bond J., Myers S., 1996, *The Astrophysical Journal Supplement Series*, **103**, 1
- Carlson J., Reid B., White M., 2013, *Monthly Notices of the Royal Astronomical Society*, **429**, 1674
- Castorina E., Paranjape A., Sheth R. K., 2016b, preprint, ([arXiv:1611.03613](https://arxiv.org/abs/1611.03613))
- Castorina E., Paranjape A., Hahn O., Sheth R. K., 2016a, preprint, ([arXiv:1611.03619](https://arxiv.org/abs/1611.03619))
- Chan K. C., Scoccimarro R., Sheth R. K., 2012, *Phys. Rev. D*, **85**, 083509
- Chan K. C., Sheth R. K., Scoccimarro R., 2015, preprint, ([arXiv:1511.01909](https://arxiv.org/abs/1511.01909))
- Chan K. C., Sheth R. K., Scoccimarro R., 2016, In preparation
- Crocce M., Fosalba P., Castander F. J., Gaztañaga E., 2010, *Monthly Notices of the Royal Astronomical Society*, **403**, 1353
- Dalal N., White M., Bond J. R., Shirokov A., 2008, *The Astrophysical Journal*, **687**, 12
- Desjacques V., Smith R. E., 2008, *Physical Review D*, **78**, 023527
- Desjacques V., Crocce M., Scoccimarro R., Sheth R. K., 2010, *Phys. Rev. D*, **82**, 103529
- Desjacques V., Jeong D., Schmidt F., 2016, preprint, ([arXiv:1611.09787](https://arxiv.org/abs/1611.09787))
- Despali G., Giocoli C., Angulo R. E., Tormen G., Sheth R. K., Baso G., Moscardini L., 2016, *Monthly Notices of the Royal Astronomical Society*, **456**, 2486
- Feng Y., Modi C., 2016, preprint, ([arXiv:1607.03224](https://arxiv.org/abs/1607.03224))
- Feng Y., Chu M.-Y., Seljak U., 2016, preprint, ([arXiv:1603.00476](https://arxiv.org/abs/1603.00476))
- Fry J. N., Gaztanaga E., 1993, *The Astrophysical Journal*, **413**, 447
- Fujita T., Mauerhofer V., Senatore L., Vlah Z., Angulo R., 2016, preprint, ([arXiv:1609.00717](https://arxiv.org/abs/1609.00717))
- Gil-Marín H., Noreña J., Verde L., Percival W. J., Wagner C., Manera M., Schneider D. P., 2015, *Monthly Notices of the Royal Astronomical Society*, **451**, 539
- Hamaus N., Seljak U., Desjacques V., Smith R. E., Baldauf T., 2010, *Physical Review D*, **82**, 043515
- Hoffmann K., Bel J., Gaztañaga E., 2015, *Monthly Notices of the Royal Astronomical Society*, **450**, 1674
- Hoffmann K., Bel J., Gaztanaga E., 2016, preprint, ([arXiv:1607.01024](https://arxiv.org/abs/1607.01024))
- Kaiser N., 1984, *ApJ*, **284**, L9
- Kaiser N., Cole S., 1989, in Frenk C. S., Ellis R. S., Shanks T., Heavens A. R., Peacock J. A., eds, *NATO Advanced Science*

Institutes (ASI) Series C Vol. 264, NATO Advanced Science
Institutes (ASI) Series C. p. 243

Lazeyras T., Wagner C., Baldauf T., Schmidt F., 2016, *J. Cosmology Astropart. Phys.*, **2**, 018

Li Y., Hu W., Takada M., 2016, *Phys. Rev. D*, **93**, 063507

Ludlow A. D., et al., 2013, *Monthly Notices of the Royal Astronomical Society*, **432**, 1103

Matsubara T., 2008, *Phys. Rev. D*, **78**, 083519

McDonald P., 2003, *The Astrophysical Journal*, **585**, 34

McDonald P., Roy A., 2009, *Journal of Cosmology and Astroparticle Physics*, 2009, 020

Mirbabayi M., Schmidt F., Zaldarriaga M., 2015, *J. Cosmology Astropart. Phys.*, **7**, 030

Mo H., White S. D., 1996, *Monthly Notices of the Royal Astronomical Society*, **282**, 347

Musso M., Sheth R. K., 2012, *Monthly Notices of the Royal Astronomical Society*, **423**, L102

Musso M., Paranjape A., Sheth R. K., 2012, *Monthly Notices of the Royal Astronomical Society*, **427**, 3145

Paranjape A., Sheth R. K., Desjacques V., 2013a, *Monthly Notices of the Royal Astronomical Society*, p. stt267

Paranjape A., Sefusatti E., Chan K. C., Desjacques V., Monaco P., Sheth R. K., 2013b, *Monthly Notices of the Royal Astronomical Society*, **436**, 449

Robertson B. E., Kravtsov A. V., Tinker J., Zentner A. R., 2009, *The Astrophysical Journal*, **696**, 636

Saito S., Baldauf T., Vlah Z., Seljak U., Okumura T., McDonald P., 2014, *Physical Review D*, **90**, 123522

Sánchez A. G., et al., 2017, *Monthly Notices of the Royal Astronomical Society*, **464**, 1640

Seljak U., Warren M. S., 2004, *Monthly Notices of the Royal Astronomical Society*, **355**, 129

Senatore L., 2015, *J. Cosmology Astropart. Phys.*, **11**, 007

Sheth R. K., Tormen G., 1999, *Monthly Notices of the Royal Astronomical Society*, **308**, 119

Sheth R. K., Mo H. J., Tormen G., 2001, *Monthly Notices of the Royal Astronomical Society*, **323**, 1

Sheth R. K., Chan K. C., Scoccimarro R., 2013, *Phys. Rev. D*, **87**, 083002

Sirko E., 2005, *The Astrophysical Journal*, **634**, 728

Szalay A. S., 1988, *The Astrophysical Journal*, **333**, 21

Tinker J., Kravtsov A. V., Klypin A., Abazajian K., Warren M., Yepes G., Gottlöber S., Holz D. E., 2008, *The Astrophysical Journal*, **688**, 709

Tinker J. L., Robertson B. E., Kravtsov A. V., Klypin A., Warren M. S., Yepes G., Gottlöber S., 2010, *The Astrophysical Journal*, **724**, 878

Vlah Z., Castorina E., White M., 2016, preprint, ([arXiv:1609.02908](https://arxiv.org/abs/1609.02908))

Wagner C., Schmidt F., Chiang C.-T., Komatsu E., 2015, *Monthly Notices of the Royal Astronomical Society*, **448**, L11

Wang L., Reid B., White M., 2014, *Monthly Notices of the Royal Astronomical Society*, **437**, 588

Watson W. A., Iliev I. T., D'Aloisio A., Knebe A., Shapiro P. R., Yepes G., 2013, *Monthly Notices of the Royal Astronomical Society*, **433**, 1230

White M., Reid B., Chuang C.-H., Tinker J. L., McBride C. K., Prada F., Samushia L., 2015, *Monthly Notices of the Royal Astronomical Society*, **447**, 234

APPENDIX A: THIRD ORDER BIAS

In principle, we should be able to extend the above estimates to higher order bias parameters. In this appendix, we provide details on our attempts to do so. For the real space estimates, this involves calculating the mean of third

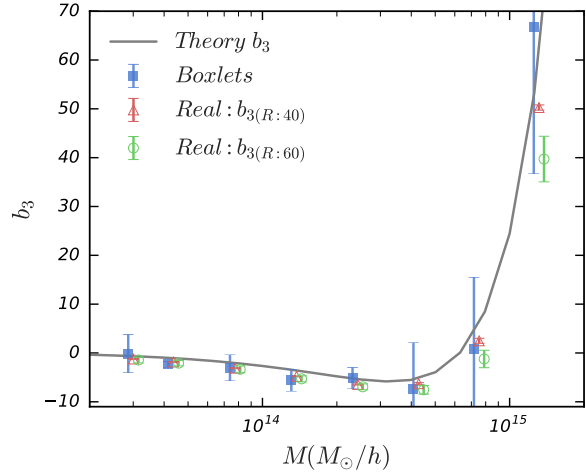


Figure A1. $b_3(M)$ from real space and PBS: The trend qualitatively agrees with the theory but PBS measurements have significant error bars.

Hermite polynomial at the position of the halos, which is straightforward. Our attempts to extend the Fourier space estimate return very noisy estimates for b_3 on large scales. This is due to $P_{h\delta}$ & $P_{h\delta^3}$ as well as $P_{\delta\delta}$, $P_{\delta^3\delta}$ & $P_{\delta^3\delta^3}$ being degenerate on large scales.

In the PBS case however, we can simply fit for following equation:

$$\delta_h(\mathbf{x}) = b_1\delta(\mathbf{x}) + \frac{b_2}{2}\delta^2(\mathbf{x}) + \frac{b_3}{6}\delta^3(\mathbf{x}) + b_s s^2(\mathbf{x}) \quad (\text{A1})$$

The results for various estimates are shown in Figure A1, where we are showing the real space results only from $3 \text{ Gpc}/h$, to compare them with their separate universe counterparts. While the numbers generally agree, the error bars are quite big in the PBS case.